land

MDPI

Article

Responses of Soil Infiltration to Water Retention Characteristics, Initial Conditions, and Boundary Conditions

Lesheng An [1], Kaihua Liao [2,*] and Chun Liu [1]

[1] School of Resources and Environment, Anqing Normal University, Anqing 246133, China; als00316@163.com (L.A.); yixiang0302@126.com (C.L.)
[2] Key Laboratory of Watershed Geographic Sciences, Nanjing Institute of Geography and Limnology, Chinese Academy of Sciences, Nanjing 210008, China
* Correspondence: khliao@niglas.ac.cn; Tel.: +86-25-86882139

Abstract: (1) Background: Simulation of soil water infiltration process and analysis of its influencing factors are important for water resources management. (2) Methods: In this study, the relative contributions of the soil water retention characteristics (SWRC) estimation, initial water content, and constant pressure head at upper boundary to the cumulative infiltration under various soil conditions were quantified based on the 1-D Richards' equation and 900 scenarios. Scenario simulations were performed for two SWRC estimation methods (Jensen method and Rosetta); three different initial water contents (0.15, 0.20, and 0.25 cm^3/cm^3); five different constant pressure heads (0.5, 1, 2, 4, and 8 cm); and thirty soil samples with varying texture and bulk density. (3) Results: Rosetta representing the drying branch of the SWRC yielded higher simulated cumulative infiltration compared with the Jensen method representing the wetting branch of the SWRC. However, the Jensen method–predicted cumulative infiltration fluxes matched well with the measured values with a low RMSE of 0.80 cm. (4) Conclusions: The relative contribution of the SWRC estimation method to cumulative infiltration (19.1–72.2%) was compared to that of constant pressure head (14.0–65.5%), and generally greater than that of initial water content (2.2–29.9%). Findings of this study have practical significance for investigating the transport of water, nutrients, and contaminants in the unsaturated zone.

Keywords: soil infiltration; Jensen method; Rosetta; 1-D Richards' equation

Citation: An, L.; Liao, K.; Liu, C. Responses of Soil Infiltration to Water Retention Characteristics, Initial Conditions, and Boundary Conditions. *Land* **2021**, *10*, 361. https://doi.org/10.3390/land10040361

Academic Editor: Chiara Piccini

Received: 27 February 2021
Accepted: 23 March 2021
Published: 1 April 2021

1. Introduction

Knowledge of the soil water infiltration process is important for the management of water resources across spatio-temporal scale [1]. For example, urban development causes water losses. Some of them can have a substantial effect on the catchment, including soil drought. To estimate water losses due to urbanization, we need to know the process of water infiltration [2–4]. In addition, water infiltration has a substantial influence on availability of water and nutrients for plants, microbial activity, and chemical weathering [5,6]. In the 20th century, numerous models were established to study the process of soil infiltration, such as Richards' equation [7], the Green–Ampt model [8], the Philip model, and the Horton model [9,10]. Richards' equation had rigorous physical basis since this model was derived based on the Darcy–Buckingham Law and mass conservation for water movement in unsaturated soils [11]. Therefore, it has been often applied as a reference to test the accuracy of the other infiltration models [12–14].

Analytical solutions of Richards' equation require the soil water retention curve (SWRC), which relates pressure head and soil water content. Soil water infiltration has been widely reported to be influenced by the SWRC, which is closely related to basic soil properties (e.g., texture and bulk density) [15]. However, direct measurement of the SWRC is time consuming and laborious [16]. Pedotransfer functions (PTFs) (e.g., Rosetta) were often used to predict the SWRC from easily measurable soil properties [17]. For example, Liao et al. [18] applied PTFs to assess the SWRCs and their spatial variability in

Qingdao City, China. Minasny et al. [19] used artificial neural networks (ANNs) coupled with bootstrap aggregation to predict the SWRC and hydraulic conductivities. However, the majority of PTFs were developed to estimate the drying branch of the SWRC and neglected the wetting branch of the curve. The hysteresis phenomenon was always found when measuring the SWRC in laboratory [20–22]. Recently, Jensen et al. [23] proposed a theoretical approach to predict the drying branch of the SWRC from soil texture.

Richards' equation can be solved analytically with simple geometric condition as well as initial and boundary conditions [24,25]. Previous studies have found that soil infiltration was influenced by the initial water content. For example, Hino et al. [26] indicated that the loss of infiltrated rainfall was significantly correlated with the initial water content when it does not exceed the infiltration rate of the soil. Leuther et al. [27] found that the infiltration front stability is dependent on the initial water content of the soil from two orchards in Israel. In addition, the boundary condition was also found to affect the water infiltration of soil in previous studies. As reported by Feng et al. [28], the higher water ponding depth at the soil surface induced a monotonic increase in infiltration rate for a water-repellent sand. A similar result was also observed by Hsu et al. [29] for prewetted sand columns. In this case, the relative impact of the SWRC estimation on the soil infiltration may rely on the settings of the initial and boundary conditions. Previous studies mostly considered only one or two factors affecting soil infiltration (e.g., Hsu et al. [29], Lassabatere et al. [30], and Bughici and Wallach [31]). Only a few studies assessed the coupling effects of multiple factors on soil infiltration. For example, Gong et al. [15] evaluated the coupling effects of surface charges, adsorbed counterions, and grain-size distribution on soil water infiltration. However, the response of soil infiltration to the interactions among the SWRC estimation, initial water content, and boundary condition has been rarely investigated.

The objectives of this study were to (i) compare the Jensen method– and Rosetta-predicted SWRC for simulating soil infiltration process based on an indoor downward water infiltration experiment in a soil column and (ii) quantify the relative contributions of the SWRC estimation, initial water content, and boundary condition to soil infiltration based on scenario analysis, with consideration of various soil conditions.

2. Materials and Methods

2.1. Soil Data Resources

Thirty soil samples were selected from the Unsaturated Soil Hydraulic Database (UNSODA) database [32] (Table 1). The soil particle-size distribution, organic matter content (OMC), and bulk density (BD) of the 30 soils were provided. The modified logistic growth (MLG) model was applied to obtain the full description of soil particle-size distribution [33]:

$$W = 1/(1 + a * \exp(-b * D^c)), \quad (1)$$

where W is the cumulative weight percentage (%) corresponding to particle diameter D (μm), and a, b and c are empirical parameters. Figure 1 shows that the predicted cumulative grain-size distribution by using the MLG model matched well with the measured one. The clay (<0.002 mm), silt (0.002–0.05 mm), fine sand (0.05–0.5 mm), and coarse sand contents (0.5–2 mm) of each soil sample were then determined. From Table 1, the BD, OMC, coarse sand, fine sand, silt, and clay contents ranged between 0.72–1.81 g/cm^3, 0.00–5.60%, 0.00–80.00%, 4.40–100.00%, 0.00–55.91%, and 0.00–62.00%, respectively, indicating a large discrepancy among different samples. In addition, it was also found that the content of organic matter in soil with low BD was generally higher [34].

Table 1. Basic soil properties of the 30 soil samples selected from the Unsaturated Soil Hydraulic Database UNSODA.

Soil Code	Bulk Density (g/cm^3)	Organic Matter (%)	Coarse Sand (%)	Fine Sand (%)	Silt (%)	Clay (%)
SC1010	1.64	0.01	7.90	75.10	14.00	3.00
SC1011	1.52	-	7.30	75.20	14.50	3.00
SC1012	1.40	-	9.50	73.00	15.00	2.50
SC1013	1.49	-	8.00	77.00	13.00	2.00
SC1014	1.53	-	8.40	78.60	11.00	2.00
SC1015	1.72	-	8.30	73.70	12.00	6.00
SC1020	1.61	-	80.00	10.00	5.50	4.50
SC1021	1.58	-	72.00	17.00	5.00	6.00
SC1022	1.60	-	76.30	13.00	6.40	4.30
SC1023	1.67	-	78.40	15.60	4.00	2.00
SC1024	1.68	-	72.30	22.70	3.00	2.00
SC1030	1.48	1.70	8.60	70.40	13.70	7.30
SC1031	1.48	0.20	9.30	69.70	13.20	7.80
SC1032	1.53	0.10	11.00	69.00	12.20	7.80
SC1041	1.51	0.78	7.50	85.50	5.00	2.00
SC1300	1.26	-	0.03	38.81	29.77	31.40
SC1301	1.27	-	0.03	38.81	29.77	31.40
SC1310	1.60	-	0.00	95.60	2.40	2.00
SC1410	1.41	-	0.00	100.00	0.00	0.00
SC2020	0.72	5.60	0.00	4.40	33.60	62.00
SC2021	0.89	5.60	0.00	4.40	33.60	62.00
SC2022	0.75	5.60	0.00	4.40	33.60	62.00
SC2310	1.71	-	9.99	89.29	0.72	0.01
SC3340	1.41	0.89	16.01	81.81	2.17	0.02
SC4690	1.32	-	0.06	23.31	54.83	21.80
SC4700	1.28	-	0.08	11.21	55.91	32.79
SC4710	1.28	-	0.01	50.69	37.79	11.51
SC4720	1.48	-	8.90	82.61	8.49	0.00
SC4940	1.76	-	38.02	35.11	0.57	26.30
SC4941	1.81	-	40.90	31.13	0.27	27.70

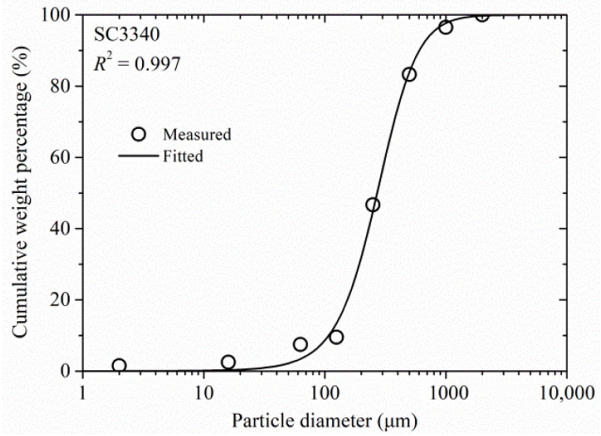

Figure 1. Measured and predicted cumulative grain-size distribution curve for soil sample with a code of 3340 (SC3340) by using the modified logistic growth model.

2.2. The Jensen Method

Jensen et al. [23] developed a theoretical approach to predict the drying branch of the SWRC from texture by scaling volumetric particle fractions to pore volume fractions. The reason is that there is a similar shape between the particle-size distribution and the SWRC [35]. They proposed five functions for water contents at pF 1.7, 2.0, 2.2, 2.7, and 3.0.

Recently, Liao et al. [36] further modified the Jensen method for estimating the wetting branch of the SWRC. For pF 1.7, 2.0, and 2.2, the functions of water contents are expressed as

$$\theta(\Psi) = \omega\ \theta_s\ (1 - (V_{CS} + \beta_1\ V_{FS}) * (V_{CS} + V_{FS})), \quad (2)$$

where ω is an empirical parameter, θ_s is the saturated water content, V_{CS} and V_{FS} are the relative volume coarse sand and fine sand, respectively, and β_1 is a parameter reflecting the water filling degree of the pores of the fine sand fraction. For pF 2.7 and 3.0, the functions of water contents are obtained:

$$\theta(\Psi) = \omega\ \theta_s\ (1 - (V_{CS} + \beta_1\ V_{FS} + \beta_2\ V_S) * (V_{CS} + V_{FS} + V_S)), \quad (3)$$

where vs. is the relative volume silt, and β_2 is a parameter reflecting the water filling degree of the pores of the silt fraction. The ω and β_1 values ranged between 0.63–0.72 and 0.87–0.96 for the five pF values, respectively, while the β_2 value equaled to 1 at pF 2.7 and 3.0. The obtained five data pairs of pressure head and water content were then used to parameterize the van Genuchten [20] model to predict the continuous wetting branch of the SWRC. The van Genuchten model is given as

$$\theta(h) = \theta_r + (\theta_s - \theta_r)/[1 + (\alpha\ h)^{\ n}]^{\ (1 - 1/n)}, \quad (4)$$

where θ_r is the residual water content (cm^3/cm^3), and α and n are shape-defining parameters.

Rosetta implemented five hierarchical PTFs for the estimation of SWRC [17]. The hierarchical in PTFs allowed the estimation of van Genuchten model parameters using limited (textural classes only) to more extended (texture, BD, and one or two water retention points) input data. Rosetta was based on ANN analyses combined with the bootstrap method, thus allowing the program to provide uncertainty estimates of the predicted SWRC. In this study, for a comparison purpose, the soil water retention parameters were predicted with both the modified Jensen method [36] (representing the wetting branch of the SWRC) and the Rosetta software [17] (representing the drying branch of the SWRC) using particle-size distribution and bulk density.

2.3. Soil Water Infiltration Experiment

An indoor ponded infiltration experiment was performed in a single vertical column of uniformly packed loam passed through a 2 mm sieve. The soil BD, OMC, coarse sand, fine sand, silt, and clay contents were 1.40 g/cm^3, 2.04%, 0.50%, 45.11%, 44.80%, and 9.59%, respectively. θ_s was determined as 0.372 cm^3/cm^3 using the gravimetric method, while the saturated hydraulic conductivity (K_s) was measured as 0.057 cm/min in the laboratory by variable falling head method. Figure 2 shows the sketch map of the experiment equipment. The soil column had a size of 60 cm in height and 18.3 cm in width. There were gravel layer and drainage room under the soil column. After installing the soil column, the height of the Markov bottle was then fixed to ensure ponded infiltration under the constant pressure head of 2 cm. The Markov bottle readings were recorded in the process of soil infiltration. The experiment was over when the water was overflowed from the drainage. Due to the short duration of the experiment, the effect of evaporation on soil infiltration can be neglected.

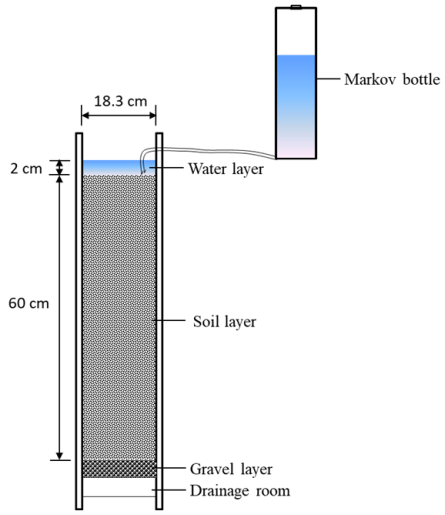

Figure 2. Sketch map of the soil water infiltration experiment equipment.

2.4. Numerical Method and Scenario Simulation

The 1-D Richards' equation was employed to simulate the soil infiltration process and can be formulated as

$$\partial\theta/\partial t = \partial/\partial z\,[K\,(\partial h/\partial z + 1)], \tag{5}$$

where t is time, z is the spatial coordinate, and K is the unsaturated hydraulic conductivity, which can be determined by the Mualem [37] model. The solution of Equation (5) requires knowledge of the initial soil profile water distribution:

$$\theta(z, t) = 0.08\ \mathrm{cm}^3/\mathrm{cm}^3\ t = 0, \tag{6}$$

The upper boundary condition is defined by the constant pressure head at the soil surface:

$$h(z, t) = 2\ \mathrm{cm}\ z = 0, t > 0, \tag{7}$$

While the lower boundary condition was defined as the free drainage at the depth of 60 cm:

$$\partial h/\partial z = 0\ z = 60\ \mathrm{cm}, t > 0, \tag{8}$$

The 1-D Richards' equation was solved by the Galerkin finite element method. In order to assess the coupling effects of the SWRC estimation, initial water content and upper boundary condition on soil infiltration with consideration of various soil conditions, a total of 900 scenarios were established: (i) 30 soil samples from the UNSODA database representing different soil conditions; (ii) two SWRC estimations (using the Jensen method and Rosetta software [17]) reflecting hysteresis impacts on soil infiltration; (iii) three initial water contents which are 0.15, 0.20, and 0.25 $\mathrm{cm}^3/\mathrm{cm}^3$, indicating the relative dry, intermediate and relatively wet conditions, respectively; and (IV) five constant pressure head values (0.5, 1, 2, 4, and 8 cm) at the upper boundary. For each soil sample, the K_s value was estimated with Rosetta using soil texture and bulk density. All scenario simulations were run with the same lower boundary condition (free drainage).

2.5. Evaluation Criteria and Contribution Rate Analysis

The performance of the model was evaluated by the coefficient of determination (R^2), the root mean squared error (RMSE). A good model will have a high R^2 and low RMSE. The multiple regression method was applied to quantify the relative contribution

rates of different influencing factors to cumulative infiltration for each soil sample. The standardized regression equation can be expressed as

$$Y_{CI} = a_1 X_1 + a_2 X_2 + a_3 X_3, \quad (9)$$

where Y_{CI} is the standardized cumulative infiltration, a_1, a_2, and a_3 are the standardized regression coefficients, and X_1, X_2, and X_3 are the standardized values of the independent variables. The classical approach of the dummy variables was used for qualitative variable, i.e., the SWRC estimation method (1 for Jensen method and 0 for Rosetta software). The relative contribution rate of each factor to cumulative infiltration (CR_i) can be calculated as

$$CR_i = |a_i| / (|a_1| + |a_2| + |a_3|) \quad (10)$$

3. Results and Discussion

3.1. Test of the Jensen Method and Rosetta Software for Simulating Soil Water Infiltration

The Jensen method and Rosetta software were tested for simulating the indoor soil infiltration process. The θ_s, θ_r, α, and n values of the soil column obtained by the Jensen method were 0.372 cm^3/cm^3, 0, 0.0408 cm^{-1}, and 1.430, respectively, while those values predicted with Rosetta were 0.370 cm^3/cm^3, 0.041 cm^3/cm^3, 0.0109 cm^{-1}, and 1.517, respectively. As expected, the Jensen method–predicted α was larger than the Rosetta-estimated value. Figure 3a shows the predicted SWRCs of the soil column by using the Jensen method and Rosetta software. A substantial difference was found between the two SWRCs, showing that the Jensen method produced lower water contents than the Rosetta at the same pressure heads. In this case, the Rosetta produced higher simulated cumulative infiltration than the Jensen method using the 1-D Richards' equation (Figure 3b). The accuracy of the Rosetta was relatively low with a relatively high RMSE of 2.49 cm. However, the Jensen method–predicted values matched well with the measured ones with a low RMSE of 0.80 cm. The positions of the wetting front at different time for the Jensen method and Rosetta software are shown in Figure 4. The wetting front obtained by the Jensen method reached the depths of 18.0, 27.6, and 40.2 cm at time t = 50, 100, and 150 min, respectively, whereas those predicted with Rosetta reached the depths of 28.2, 41.4, and 52.8 cm, respectively. As expected, the simulated wetting front by the Rosetta software advanced more rapidly than that by the Jensen method during the infiltration process.

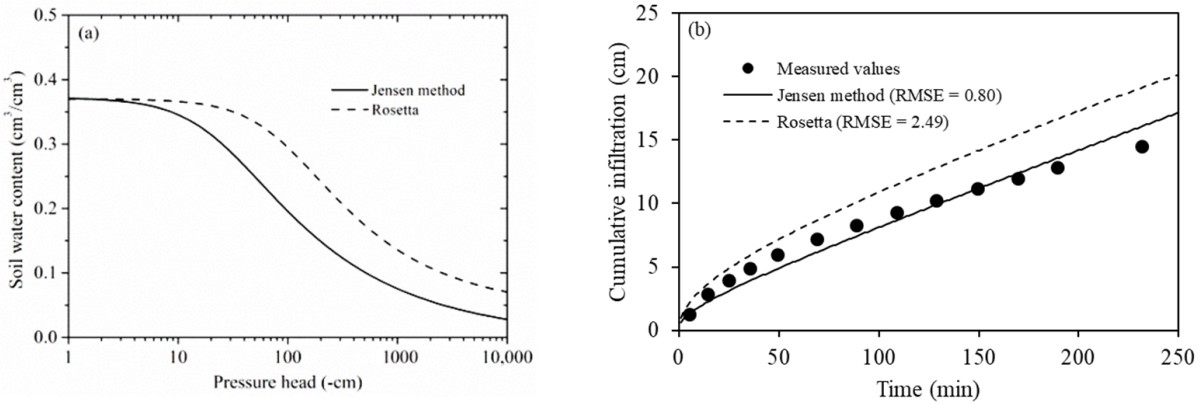

Figure 3. Comparison of the Jensen method and Rosetta software for (**a**) estimating the water retention curve of the soil column and (**b**) simulating the soil infiltration process.

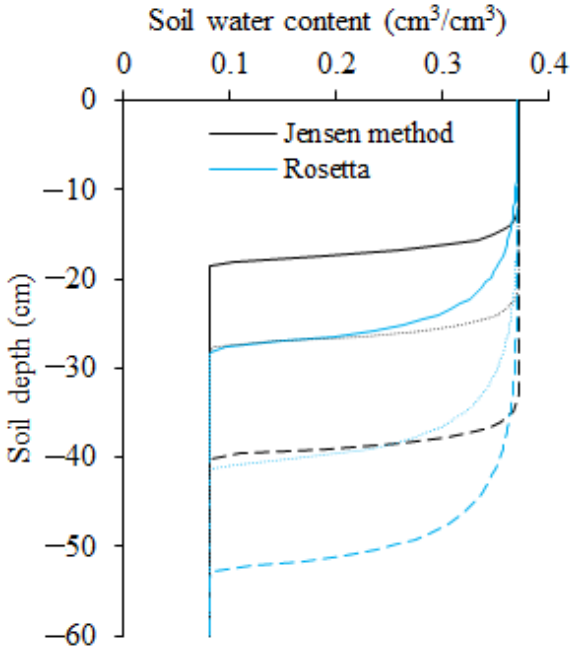

Figure 4. Comparison of the wetting front simulated by the Jensen method and Rosetta software at t = 50, 100, and 150 min after the infiltration.

Previous studies have been conducted to assess the hysteresis effect of SWRC on the water infiltration of various textured soils. Huang et al. [38] indicated that the simulation of the coarse-textured profile water content was improved during the infiltration process when hysteresis was taken into account. In the study by Abbasi et al. [39], a large difference was found between the measured fluxes and non-hysteresis-models-predicted values during the infiltration processes of the loamy and sandy loam soil. In our study, it is suggested that the Rosetta estimating the drying SWRC has to be used with caution when applying this method to simulate the infiltration process. In contrast, the Jensen method representing the wetting SWRC was demonstrated to be capable of predicting the water infiltration of the loam soil. However, this method was still needed to be validated for different textured soils.

3.2. Coupling Influences of the SWRC Estimation, Initial Water Content, and Upper Boundary Condition

Solving 1-D Richards' equation by different scenarios, 900 cumulative soil infiltration fluxes were obtained. For each soil sample, the average infiltration fluxes decreased as the increase in the initial water content (Figure 5). For example, the average of infiltration fluxes of SC1300 obtained by the Jensen method decreased from 5.62 cm to 5.20 cm as the initial water content increasing from 0.15 cm^3/cm^3 to 0.25 cm^3/cm^3. The relative contributions of various factors to cumulative soil infiltration were quantified by the regression method (Figure 6). Results indicated that initial water content had a generally lesser contribution (2.2–29.9%) to cumulative infiltration compared to the SWRC estimation method (19.1–72.2%) and constant pressure head (14.0–65.5%).

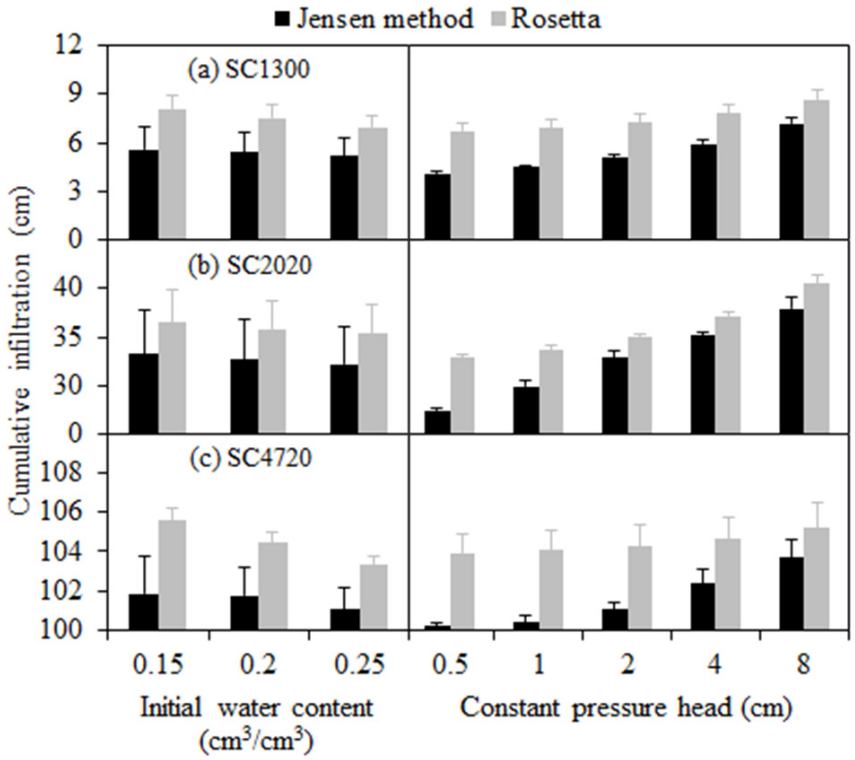

Figure 5. Average cumulative infiltration fluxes and their standard deviation (error bars) under three initial water contents and five constant pressure heads at upper boundary for soil samples with codes of (**a**) 1300, (**b**) 2020 and (**c**) 4720.

From Figure 5, the average infiltration fluxes decreased as increasing initial water content. This finding agreed with classical theory of infiltration that predicted cumulative infiltration to decrease as increases of initial water content [9]. For any SWRC prediction method, an increase in constant pressure head resulted in an increase in infiltration fluxes at any point in time. Therefore, the relationship between constant pressure head and cumulative infiltration was independent of initial water content. The above results are consistent with many previous studies [29,40,41]. In addition, SC4720 with a low OMC and clay content produced higher cumulative infiltration fluxes than SC1300 and SC2020 with a high OMC and clay content at the same initial water content and constant pressure head (Figure 5). Previous studies also observed that various soil conditions (e.g., texture, structure, and OMC) largely influenced soil infiltration and redistribution processes [42,43]. In the study by Franzluebbers [44], the stratification ratio of soil OMC (OMC at 0–3 cm depth divided by that at 6–12 cm depth) was found to control the water infiltration rate. Zhao et al. [42] indicated that a sandy loam soil can produce 23% higher infiltration than the clay and silt loam soils. Therefore, soil infiltration was synthetically affected by the static soil properties and dynamic factors (initial water content and constant pressure head). In previous studies, soil infiltration had also been demonstrated to be affected by soil properties, initial water content, and constant pressure head. For example, in the study by Camps-Roach et al. [45], the dynamic effect of the capillary pressure on water infiltration was related to the soil parameters (e.g., grain-size distributions). Hsu et al. [29] reported that the magnitude of the dynamic effect of capillary pressure depended primarily on the initial moisture content, not the constant pressure head. The results suggested that the effects of different factors on soil infiltration were dynamic and intertwined.

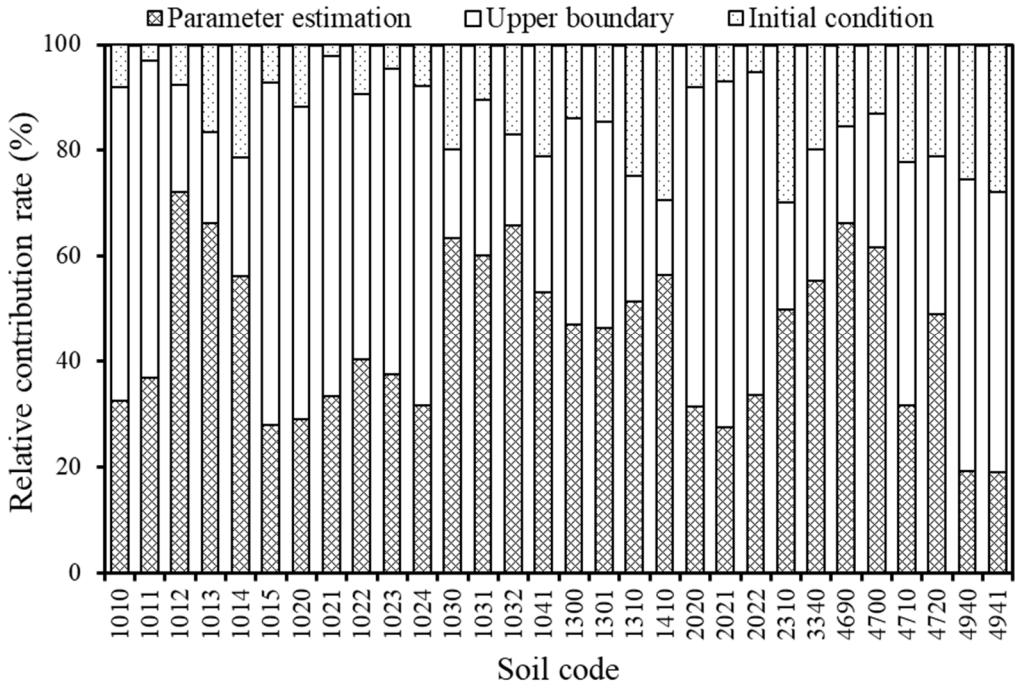

Figure 6. Relative contribution rates of different factors (parameter estimation methods, initial water contents, and constant pressure heads at upper boundary) to cumulative infiltration fluxes for the 30 soils investigated.

Influences of the SWRC estimation method, initial water content, and constant pressure head on the cumulative infiltration substantially varied under different soil conditions. Figure 7 shows the relationships between the relative contribution of the parameter estimation to soil infiltration and basic soil properties for the 30 soil samples. There was a bell-shape relationship between the relative contribution of the parameter estimation and BD, showing that the BD of 1.40 g/cm^3 corresponded to the maximum relative contribution rate. This is related to the similar relationship between the SMBE and BD. However, the relative contribution of the parameter estimation was negatively and positively correlated with the clay and fine sand contents at the 0.01 level of significance, respectively.

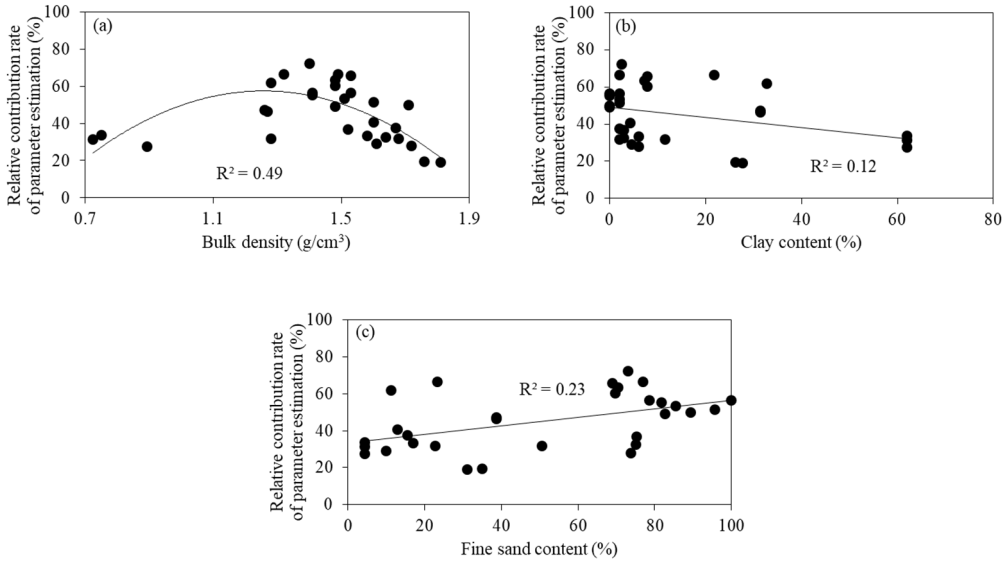

Figure 7. Relationships between the relative contribution of parameter estimation to cumulative infiltration fluxes and (**a**) bulk density, (**b**) clay, and (**c**) fine sand contents.

The relative contribution of the parameter estimation gradually increased with the soil texture from fine to coarse, yet the relative contribution of the initial and boundary conditions gradually decreased (figures not shown). The reason may be that there was a lager difference between the drying SWRC and wetting SWRC (hysteresis effect) for the coarser-textured soils than for the finer-textured soils [46]. Elmaloglou and Diamantopoulos [47] also found that the hysteresis decreased the soil leakage more in the loamy sand (6.4–10.3%) than in the silt loam (3.6–6.4%). Besides the SWRC estimation method, initial water content, and constant pressure head considered in this study, the vertical heterogeneity of soil texture greatly influenced soil infiltration as reported in the study of Zhu and Mohanty [48]. Huang et al. [38] found that the vertical change of soil texture led to the increase of water storage compared with homogeneous soil profile with similar texture. In addition, climate change and tillage conversion also affected the soil infiltration. For example, air temperature changed the soil evapotranspiration rate and soil moisture content, which in turn influenced soil infiltration [49]. Conversion from conventional tillage to conservation tillage has been demonstrated to increase saturated hydraulic conductivity and water infiltration due to greater soil organic carbon accumulation over time in conservation tillage [50,51]. Therefore, to comprehensively detect the mechanisms of the water infiltration, investigations on the coupling effects of multiple factors (e.g., vertical change of soil texture and hydraulic properties, climate change, and tillage conversion) on soil infiltration under different land use types (e.g., farmland and garden) are still needed for future research.

4. Conclusions

This study compared the derived theoretical functions and Rosetta software for estimating the wetting SWRC of the 30 soil samples from UNSODA and for simulating the infiltration process of a loam soil using a downward infiltration experiment. The Jensen method was found to have better performance in estimating the wetting SWRC and simulating the cumulative infiltration than the Rosetta software in terms of RMSE. The 1-D Richards' equation and scenario simulation were used to quantify the response of cumulative infiltration to the coupling interactions among SWRC estimation method, initial water content and constant pressure head.

As expected, an increase in constant pressure head resulted in an increase in the cumulative infiltration. The cumulative infiltration decreased as the initial water content increased. The SWRC estimation method and constant pressure head had a generally greater contribution to cumulative infiltration than initial water content. The relative contribution of the SWRC estimation to infiltration had a bell-shape relationship with the BD and a significant ($p < 0.01$) linear relationship with the clay and fine sand contents. This indicated that influences of the SWRC estimation method on the cumulative infiltration largely depended on the soil condition. The above results suggest that more efforts need to be made to obtain a high-precision SWRC and accurately describe the upper boundary conditions in the simulation of soil infiltration process.

Author Contributions: Conceptualization, L.A. and K.L.; methodology, L.A. and K.L.; software, L.A., C.L. and K.L.; formal analysis, L.A. and K.L.; data curation, L.A. and K.L.; writing—original draft preparation, L.A. and K.L.; writing—review and editing, L.A., C.L. and K.L.; funding acquisition, L.A. and K.L. All authors have read and agreed to the published version of the manuscript.

Funding: This study was funded by the National Natural Science Foundation of China, grant number 41771107; the Anhui Provincial Natural Science Foundation, grant number 1808085MD101; the Outstanding Young Talents Support Program in Universities of Anhui Province in 2020, grant number gxyq2020030; and the Youth Innovation Promotion Association, Chinese Academy of Sciences, grant number 2020317.

Institutional Review Board Statement: Not applicable.

Informed Consent Statement: Not applicable.

Data Availability Statement: Not applicable.

Conflicts of Interest: The authors declare no conflict of interest.

References

1. Herrada, M.A.; Gutiérrez-Martin, A.; Montanero, J.M. Modeling infiltration rates in a saturated/unsaturated soil under the free draining condition. *J. Hydrol.* **2014**, *515*, 10–15. [CrossRef]
2. Lepeška, T.; Wojkowski, J.; Wałęga, A.; Młyński, D.; Radecki-Pawlik, A.; Olah, B. Urbanization—Its hidden impact on water losses: Prądnik River Basin, Lesser Poland. *Water* **2020**, *12*, 1958. [CrossRef]
3. Su, W.; Gu, C.; Yang, G.; Chen, S.; Zhen, F. Measuring the impact of urban sprawl on natural landscape pattern of the Western Taihu Lake watershed, China. *Landsc. Urban Plan.* **2010**, *95*, 61–67. [CrossRef]
4. Su, W.; Ma, L.; Chen, S.; Yang, G. Conflict analysis and system optimization of urban ecological space. *J. Nat. Resour.* **2020**, *35*, 601–613.
5. Castellini, M.; Stellacci, A.M.; Sisto, D.; Iovino, M. The mechanical impact of water affected the soil physical quality of a loam soil under minimum tillage and no-tillage: An assessment using Beerkan multi-height runs and BEST-procedure. *Land* **2021**, *10*, 195. [CrossRef]
6. Suprayogo, D.; van Noordwijk, M.; Hairiah, K.; Meilasari, N.; Rabbani, A.L.; Ishaq, R.M.; Widiando, W. Infiltration-friendly agroforestry land uses on Volcanic slopes in the Rejoso Watershed, East Java, Indonesia. *Land* **2020**, *9*, 240. [CrossRef]
7. Ross, P.J. Efficient numerical methods for infiltration using Richards' equation. *Water Resour. Res.* **1990**, *26*, 279–290. [CrossRef]
8. Green, W.H.; Ampt, G.A. Studies on soil physics: 1. Flow of air and water through soils. *J. Agric. Sci.* **1911**, *4*, 1–24.
9. Philip, J.R. The theory of infiltration: 1, The infiltration equation and its solution. *Soil Sci.* **1957**, *83*, 345–357. [CrossRef]
10. Horton, R.E. The role of infiltration in the hydrologic cycle. *Trans. Am. Geophys. Union* **1933**, *14*, 446–460. [CrossRef]
11. Botros, F.E.; Onsoy, Y.S.; Ginn, T.R.; Harter, T. Richards equation-based modeling to estimate flow and nitrate transport in a deep Alluvial vadose zone. *Vadose Zone J.* **2012**, 11. [CrossRef]
12. Hsu, S.M.; Ni, C.F.; Hung, P.F. Assessment of three infiltration formulas based on model fitting and Richards equation. *J. Hydrol. Eng.* **2002**, *7*, 373–379. [CrossRef]
13. Smith, R.E. *Infiltration Theory for Hydrologic Application*; American Geophysical Union: Washington, DC, USA, 2002; Volume 15.
14. Su, N. Theory of infiltration: Infiltration into swelling soils in a material coordinate. *J. Hydrol.* **2010**, *395*, 103–108. [CrossRef]
15. Gong, Y.; Tian, R.; Li, H. Coupling effects of surface charges, adsorbed counterions and particle-size distribution on soil water infiltration and transport. *Eur. J. Soil Sci.* **2018**, *69*, 1008–1017. [CrossRef]
16. Liao, K.; Zhou, Z.; Li, Y.; Lai, X.; Zhu, Q.; Shan, N. Comparison of seven water retention functions used for modelling soil hydraulic conductivity due to film flow. *Soil Use Manag.* **2018**, *34*, 370–379. [CrossRef]
17. Schaap, M.G.; Leij, F.J.; van Genuchten, M.T. ROSETTA: A computer program for estimating soil hydraulic parameters with hierarchical pedotransfer functions. *J. Hydrol.* **2001**, *251*, 163–176. [CrossRef]
18. Liao, K.; Xu, S.; Wu, J.; Ji, S.; Lin, Q. Assessing soil water retention characteristics and their spatial variability using pedotransfer functions. *Pedosphere* **2011**, *21*, 413–422. [CrossRef]
19. Minasny, B.; Hopmans, J.W.; Harter, T.; Eching, S.O.; Tuli, A.; Denton, M.A. Neural networks prediction of soil hydraulic functions for alluvial soils using multistep outflow data. *Soil Sci. Soc. Am. J.* **2004**, *68*, 417–429. [CrossRef]
20. Van Genuchten, M.T. A closed-form equation for predicting the hydraulic conductivity of unsaturated soils. *Soil Sci. Soc. Am. J.* **1980**, *44*, 892–898. [CrossRef]
21. Braddock, R.D.; Parlange, J.Y.; Lee, H. Application of a soil water hysteresis model to simple water retention curves. *Transp. Porous Med.* **2001**, *44*, 407–420. [CrossRef]
22. Lourenço, S.D.N.; Jones, N.; Morley, C.; Doerr, S.H.; Bryant, R. Hysteresis in the soil water retention of a sand–clay mixture with contact angles lower than ninety degrees. *Vadose Zone J.* **2015**, *14*, 1–8. [CrossRef]
23. Jensen, D.K.; Tuller, M.; de Jonge, L.W.; Arthur, E.; Moldrup, P. A new two-stage approach to predicting the soil water characteristic from saturation to oven-dryness. *J. Hydrol.* **2015**, *521*, 498–507. [CrossRef]
24. Tracy, F.T. Clean two and three-dimensional analytical solutions of Richards' equation for testing numerical solvers. *Water Resour. Res.* **2006**, *42*, 1–11. [CrossRef]
25. Chen, X.; Liang, X.; Xia, J.; She, D. Impact of lower boundary condition of Richards' equation on water, energy, and soil carbon based on coupling land surface and biogeochemical models. *Pedosphere* **2018**, *28*, 497–510. [CrossRef]
26. Hino, M.; Odaka, Y.; Nadaoka, K.; Sato, A. Effect of initial soil moisture content on the vertical infiltration process—A guide to the problem of runoff-ratio and loss. *J. Hydrol.* **1988**, *102*, 267–284. [CrossRef]
27. Leuther, F.; Weller, U.; Wallach, R.; Vogel, H.J. Quantitative analysis of wetting front instabilities in soil caused by treated waste water irrigation. *Geoderma* **2018**, *319*, 132–141. [CrossRef]
28. Feng, G.L.; Letey, J.; Wu, L. Water ponding depths affect temporal infiltration rates in a water-repellent sand. *Soil Sci. Soc. Am. J.* **2001**, *65*, 315–320. [CrossRef]
29. Hsu, S.Y.; Huang, V.; Park, S.W.; Hilpert, M. Water infiltration into prewetted porous media: Dynamic capillary pressure and Green-Ampt modeling. *Adv. Water Resour.* **2017**, *106*, 60–67. [CrossRef]
30. Lassabatere, L.; Loizeau, S.; Angulo-Jaramillo, R.; Winiarski, T.; Rossier, Y.; Delolme, C.; Gaudet, J.P. Influence of the initial soil water content on Beerkan water infiltration experiments. *Geophys. Res. Abstr.* **2012**, *14*, 2278.

31. Bughici, T.; Wallach, R. Formation of soil–water repellency in olive orchards and its influence on infiltration pattern. *Geoderma* **2016**, *262*, 1–11. [CrossRef]
32. Nemes, A.; Schaap, M.G.; Leij, F.J.; Wösten, J.H.M. Description of the unsaturated soil hydraulic database UNSODA version 2.0. *J. Hydrol.* **2001**, *251*, 151–162. [CrossRef]
33. Thornley, J.H.M.; Johnson, I.R. *Plant and Crop Modelling: A Mathematical Approach to Plant and Crop Physiology*; Clarendon: Oxford, UK, 1990.
34. Alexander, E.B. Bulk densities of California soils in relation to other soil properties. *Soil Sci. Soc. Am. J.* **1980**, *44*, 689–692. [CrossRef]
35. Arya, L.M.; Paris, J.F. A physicoempirical model to predict the soil-moisture characteristic from particle-size distribution and bulk-density data. *Soil Sci. Soc. Am. J.* **1981**, *45*, 1023–1030. [CrossRef]
36. Liao, K.; Lai, X.; Jiang, S.; Zhu, Q. Estimating the wetting branch of the soil water retention curve from grain-size fractions. *Eur. J. Soil Sci.* **2020**, 1–6. [CrossRef]
37. Mualem, Y. A new model predicting the hydraulic conductivity of unsaturated porous media. *Water Resour. Res.* **1976**, *12*, 513–522. [CrossRef]
38. Huang, M.; Barbour, S.L.; Elshorbagy, A.; Zettl, J.D.; Si, B.C. Infiltration and drainage processes in multilayered coarse soils. *Can. J. Soil Sci.* **2011**, *91*, 169–183. [CrossRef]
39. Abbasi, F.; Javaux, M.; Vanclooster, M.; Feyen, J. Estimating hysteresis in the soil water retention curve from monolith experiments. *Geoderma* **2012**, *189*, 480–490. [CrossRef]
40. Warrick, A.W.; Zerihun, D.; Sanchez, C.A.; Furman, A. Infiltration under variable ponding depths of water. *J. Irrig. Drain. Eng.* **2005**, 131. [CrossRef]
41. Zhang, G.; Feng, G.; Li, X.; Xie, C.; Pi, X. Flood effect on groundwater recharge on a typical silt loam soil. *Water* **2017**, *9*, 523. [CrossRef]
42. Zhao, L.T.; Gray, D.M.; Toth, B. Influence of soil texture on snowmelt infiltration into frozen soils. *Can. J. Soil Sci.* **2002**, *82*, 75–83. [CrossRef]
43. Lai, X.; Liao, K.; Feng, H.; Zhu, Q. Responses of soil water percolation to dynamic interactions among rainfall, antecedent moisture and season in a forest site. *J. Hydrol.* **2016**, *540*, 565–573. [CrossRef]
44. Franzluebbers, A.J. Water infiltration and soil structure related to organic matter and its stratification with depth. *Soil Tillage Res.* **2002**, *66*, 197–205. [CrossRef]
45. Camps-Roach, G.; O'Carroll, D.M.; Newson, T.A.; Sakaki, T.; Illangasekare, T.H. Experimental investigation of dynamic effects in capillary pressure: Grain size dependency and upscaling. *Water Resour. Res.* **2010**, *46*, W08544. [CrossRef]
46. Topp, G.C. Soil water hysteresis in silt loam and clay loam soils. *Water Resour. Res.* **1971**, *7*, 914–920. [CrossRef]
47. Elmaloglou, S.; Diamantopoulos, E. Effects of hysteresis on redistribution of soil moisture and deep percolation at continuous and pulse drip irrigation. *Agric. Water Manag.* **2009**, *96*, 533–538. [CrossRef]
48. Zhu, J.; Mohanty, B.P. Spatial averaging of van Genuchten hydraulic parameters for steady state flow in heterogeneous soils. *Vadose Zone J.* **2002**, *1*, 261–272. [CrossRef]
49. Pruski, F.F.; Nearing, M.A. Climate-induced changes in erosion during the 21st century for eight U.S. locations. *Water Resour. Res.* **2002**, *38*, 1298. [CrossRef]
50. Liu, C.; Lu, M.; Cui, J.; Li, B.; Fang, C. Effects of straw carbon input on carbon dynamics in agricultural soils: A meta-analysis. *Glob. Chang. Biol. Bioenergy* **2014**, *20*, 1366–1381. [CrossRef]
51. Li, Y.; Li, Z.; Cui, S.; Jagadamma, S.; Zhang, Q. Residue retention and minimum tillage improve physical environment of the soil in croplands: A global meta-analysis. *Soil Tillage Res.* **2019**, *194*, 104292. [CrossRef]